Nanoporous Materials

High-Aspect-Ratio TiO_2 Nanotubes by Anodization of Titanium**

*Jan M. Macák, Hiroaki Tsuchiya, and Patrik Schmuki**

Nanotubular material surfaces produced by the electrochemical formation of self-organized porous structures on materials such as aluminum[1,2] and silicon[3,4] have attracted significant interest in recent years. While scientific thrust is often directed towards the elucidation of the principles of the self-organization phenomena, technological efforts target applications based on the direct use of the high surface area, for example, for sensing[5,6] or controlled catalysis,[7] exploit the optical properties in photonic crystals,[8] waveguides,[9] or in 3D arranged Bragg-stack type of reflectors.[10] The highly organized structures may be used indirectly as templates[11] for the deposition of other materials such as metals,[12] semiconductors,[13] or polymers.[14] Over the past few years, nanoporous TiO_2 structures have also been formed by electrochemical anodization of titanium.[15–17] Although several applications have been proposed,[18,19] a wider impact of these structures has been hampered by the fact that the layers could only been grown to a limiting thickness of a few hundreds of nanometers.

Herein we demonstrate for the first time how high-aspect-ratio, self-organized, TiO_2 films can be grown by tailoring the electrochemical conditions during titanium anodization.

Figure 1 shows scanning electron microscope (SEM) images of self-organized porous titanium oxide formed to a thickness of approximately 2.5 μm in 1M $(NH_4)_2SO_4$ electrolyte containing 0.5 wt.% NH_4F. From the SEM images it is evident that the self-organized regular porous structure consists of pore arrays with a uniform pore diameter of approximately 100 nm and an average spacing of 150 nm. It is also clear that pore mouths are open on the top of the layer while on the bottom of the structure the tubes are closed by presence of an about 50-nm thick barrier layer of TiO_2.

The key to achieve high-aspect-ratio growth is to adjust the dissolution rate of TiO_2 by localized acidification at the pore bottom while a protective environment is maintained along the pore walls and at the pore mouth. In our previous work in HF and NaF solutions[15,20] it was established that the thickness of the porous layer is essentially the result of an equilibrium between electrochemical formation of TiO_2 at the pore bottom and the chemical dissolution of this TiO_2 in an F^- ion containing solution (Figure 2). The solubility of TiO_2 in HF, forming $[TiF_6]^{2-}$, is essential for pore formation, however, it is also the reason that previous attempts to form porous layers in HF electrolytes always resulted in layer thicknesses in the range of some 100 nm.

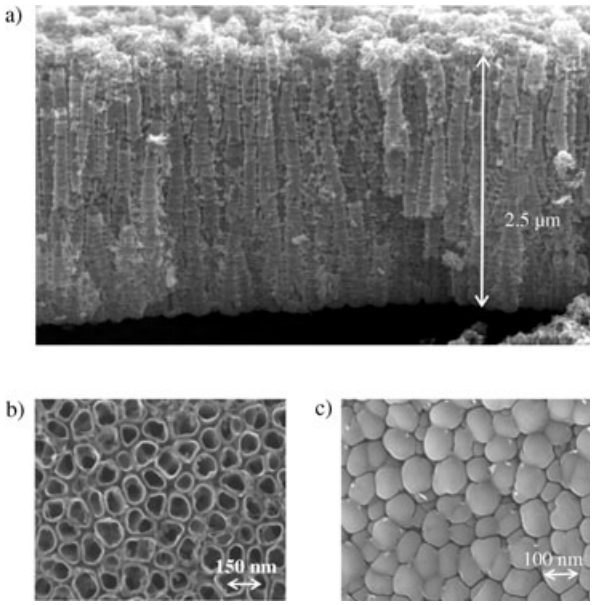

Figure 1. SEM images of porous titanium oxide nanotubes. The cross-sectional (a), top (b), and bottom (c) views of a 2.5-μm thick self-organized porous layer. The titanium sample was anodized up to 20 V in 1 M $(NH_4)_2SO_4$ + 0.5 wt.% NH_4F using a potential sweep from open-circuit potential to 20 V with sweep rate 0.1 Vs^{-1}. The average pore diameter is approximately 100 nm and the average pore spacing is approximately 150 nm.

We tackled the problem by controlling the self-induced acidification of the pore bottom that is caused by the electrochemical dissolution of the metal (Figure 2a–c). Main reason for the localized acidification is the oxidation and hydrolysis of elemental titanium [Eq. (1), in Figure 2]. The chemical dissolution rate of TiO_2 is highly dependent on the pH value (see Figure 2d). Using a numerical simulation of the relevant ion fluxes we can construct the pH profile in the pore (such as in Figure 2b), in other words, the ideal ion flux for the desired pH profile can then be determined. Furthermore we can tune the dissolution rate by the dissolution current. In other words, using a buffered neutral solution as electrolyte and adjusting the anodic current flow to an ideal value, acid can be created where it is needed, that is, at the pore bottom, while higher pH values are established at the pore mouth as a result of migration and diffusion effects of the pH buffer species (NH_4F, $(NH_4)_2SO_4$). Assuming equilibrium, the flux of dissolving species (leading to acidification at the pore bottom) and the flux of buffering species are equal. The calculations show that for the experimental conditions given in Figure 1 the pH value at the pore bottom is around 2 and increase to about 5 at the pore mouth, this corresponds to a drop in the local chemical etch rate of about 20 times.

We used a voltage-sweep technique to achieve a steady-state current and to establish the desired pH profile. The reason to use a voltage-sweep technique rather than a

[*] J. M. Macák, Dr. H. Tsuchiya, Prof. Dr. P. Schmuki
Department of Materials Science, WW4-LKO
University of Erlangen-Nuremberg
Martensstrasse 7, 91058 Erlangen (Germany)
Fax: (+49) 9131-852-7582
E-mail: schmuki@ww.uni-erlangen.de

[**] The authors would like to acknowledge A. Friedrich and H. Hildebrand for SEM and XPS investigations and L. Taveria for valuable help with the experiments.

  DOI: 10.1002/anie.200462459

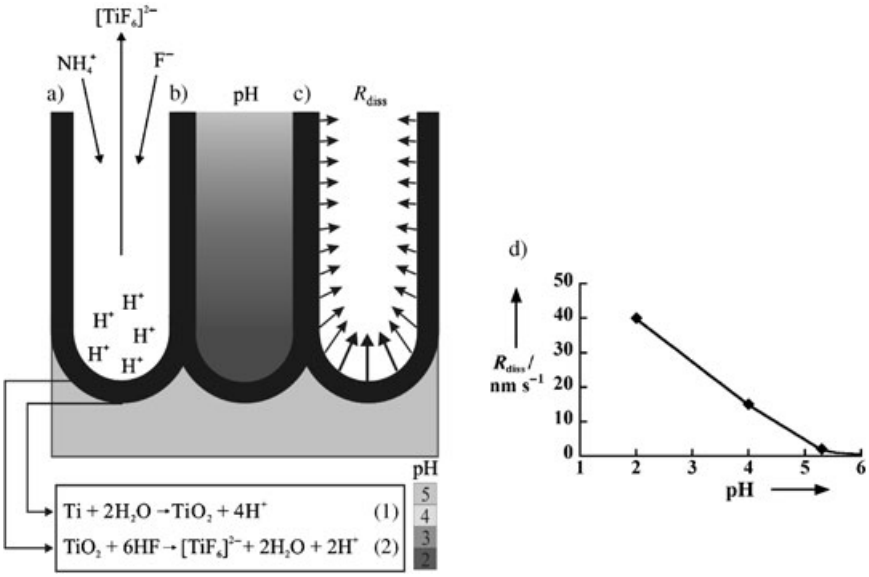

Figure 2. Tuning the electrochemical conditions to achieve high-aspect-ratio structures. Schematic representation of the dissolution reactions and mechanisms (a), the pH profile within a pore (b), the dissolution-rate profile within a pore wall (c). Experimental determination of the dissolution rate, R_{diss}, of the anodic TiO_2 depending on the pH value (d), results are taken from XPS sputter profiles of 20 V anodic oxide immersed for different times in 1 M $(NH_4)_2SO_4$ + 0.5 wt.% NH_4F solution with different pH values.

galvanostatic approach is that the system in galvanostatic mode has a tendency to oscillate, which leads to a destabilization of the steady-state situation within the pore.[21]

X-ray photoelectron spectroscopy (XPS) analysis revealed that the porous layer shown in Figure 1 consists of approximately 62 ± 5 atom% of oxygen and 38 ± 5 atom% of titanium. The Ti $2p_{3/2}$ peak was found to be at $458.5\,eV \pm 0.5\,eV$ (TiO_2 reference 458.8 eV). So evidently the porous layer consists of TiO_2. Only negligible traces of F from the electrolyte could be detected throughout the film. Depending on the applied voltage the structure of the TiO_2 film is typically reported to be either amorphous (below 20 V) or crystalline (higher voltages), where the presence of anatase, a mixture of anatase and rutile, or rutile can be observed.[22,23] X-ray diffraction analysis[21] of our structures indicated an amorphous structure that can be converted, for example, into anatase upon annealing.

Figure 3 demonstrates that the pore-formation process is indeed sensitive to the electrochemical parameters used. For example, for anodization in electrolyte containing a significantly higher NH_4F concentration (5 wt.%) and using a low sweep rate only short pores (nanotubes) are obtained (Figure 3a). Using a fast sweep rate leads to the growth of thick porous layer (Figure 3b). However, the surface in this thick porous layer is very rough and not regular and the structure itself is loosely cross-linked and not tubular.

In general, using a lower NH_4F concentration leads to the growth of regular self-organized porous tube-like structures, whereas in concentrated electrolytes the structure is rough and cross-linked. For the electrolyte used (1M $(NH_4)_2SO_4$ + 0.5 wt.% NH_4F) the diameter is slightly influenced by the sweep rate. The pore diameter changes in range of 90–110 nm and the higher the sweep rate the wider the pores. In the light of our simulations these morphological effects can be associated with the degree of acidification of the pore electrolyte during anodization, this leads to an enhanced or retarded etching of the side walls of the pores. The results thus imply that the mechanism of pore formation in this system is significantly different from the relatively well investigated aluminum case. While in aluminum, electric-field-aided ion transport through the pore bottom is the dominant mechanism (chemical oxide dissolution plays a minor role) it is evident that the chemical effects in the case of TiO_2 pore growth can become dominant.

The self-organized porous TiO_2 layers have various potential applications. For example, TiO_2 nanoparticles are extremely efficient for solar energy conversion[24] when used in dye-sensitized solar cells. These cells consist typically of a 5–10-μm thick layer of TiO_2 nanoparticles. Ordered TiO_2 nanotubes with tube lengths in this

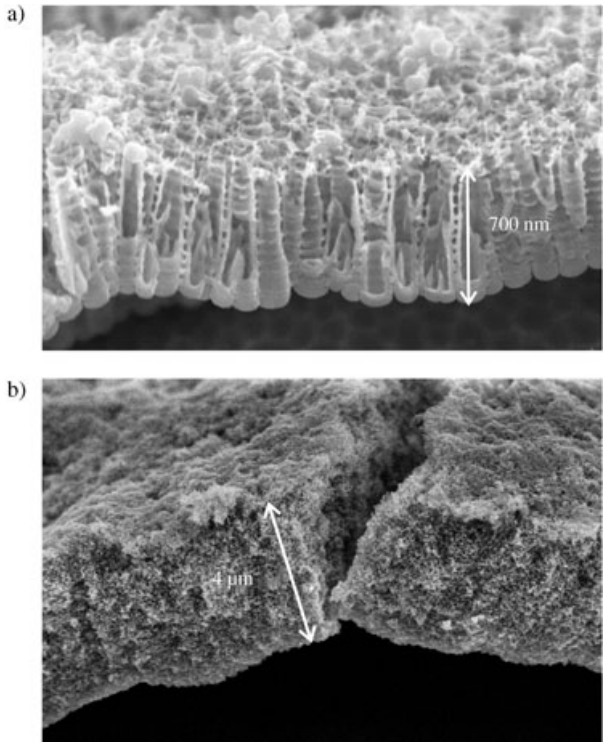

Figure 3. Anodization parameter dependence of the morphology of porous titanium oxide. Both samples were anodized in 1 M $(NH_4)_2SO_4$ + 5 wt.% NH_4F to 20 V with a low ramp speed of $10\,mV\,s^{-1}$ (a), and with a high ramp speed of $20\,V\,s^{-1}$ (b). In both cases a distinctly different thickness and morphology from that shown in Figure 1 is obtained as a result of the strongly different pH profiles in the pores.

range may give higher conversion efficiency as losses owing to grain boundaries (in the sintered nanoparticles) can be avoided. Additionally, TiO_2 shows self-cleaning properties,[25] a controllable wettability,[26] and a high degree of biocompatibility in biomedical applications,[27] for instance as a dental or hip implant (high osseointegration). It can be used for controlled catalysis of organic reactions[7] or for sensing (e.g. hydrogen[18] and oxygen[28]). Owing to its high refractive index (about 60% higher than porous alumina), the self-organized porous TiO_2 structures may be suitable for the construction of photonic crystals[29] or waveguides.[9]

In all these applications the nanotubular structures herein offer advantages: unspecified nanoparticles can be replaced by highly ordered tubes. A key advantage is that essentially any form of a titanium surface (sheets, foils, sputtered layers) can be treated in a quick and low-cost approach with a TiO_2 nanotube layer coating. However, for some applications a separation of the tube array into isolated tubes may be essential—this will be subjected to future work.

Experimental Section

Surface treatment: Titanium samples (0.1-mm thick foils, 99.6% purity, Goodfellow) were degreased by sonicating in acetone, isopropanol, and methanol, then rinsed with deionized water and dried in a nitrogen stream.

Electrochemical treatment: Titanium samples were contacted and then pressed against an O-ring in an electrochemical cell, leaving 1 cm^2 exposed to the electrolyte. The electrochemical setup consisted of a conventional three-electrode configuration with a platinum gauze as a counter electrode and a Haber–Luggin capillary with Ag/AgCl (1M KCl) reference. Electrochemical experiments were carried out at room temperature using a high-voltage potentiostat Jaissle IMP 88. The electrolyte was 1M $(NH_4)_2SO_4$ with the addition of small amounts of NH_4F (0.5–5 wt.%). All electrolytes were prepared from reagent grade chemicals and deionized water. The electrochemical treatment consisted of a potential ramp from the open-circuit potential (OCP) to 20 V with a different sweep rate followed by holding the applied potential at 20 V for different times. After the electrochemical treatment the samples were rinsed with deionized water and dried with nitrogen stream.

Numerical calculations: Finite element based calculations of the pH profiles in the tubes were performed using the approach given by Kelly et al.[30]

Surface characterization: Scanning electron microscopy using a Hitachi SEM FE 4800 was employed for the structural and morphological characterization of the porous titanium oxide. In order to gain information on thickness of the porous layer, direct SEM cross-sectional thickness measurements were carried out on mechanically bent samples, while bending the porous layer cracked into many parts and in some cases a partial lift-off of the porous layer occurred. In this way the bottom-view images of the porous layer pieces were obtained.

XPS (PHI 5600 XPS) depth profiles (by Ar^+ ion sputtering at 3.2 kV using the Ti peak at 459 eV, the O peak at 528 eV, and the F peak at 685 eV) were acquired on samples with a TiO_2 layer formed anodically at 20 V (this layer has a thickness of 50 nm) The anodic oxide layer was immersed for different times in the fluoride-containing etching solution to determine the dissolution rate of the oxide at the different pH values.

Received: October 28, 2004
Published online: February 25, 2005

Keywords: electrochemistry · nanoporous materials · nanotubes · self-organization · titanium

[1] H. Masuda, K. Fukuda, *Science* **1995**, *268*, 1466.
[2] H. Masuda, K. Fukuda, *Appl. Phys. Lett.* **1997**, *71*, 2770.
[3] L. T. Canham, *Appl. Phys. Lett.* **1990**, *57*, 1046.
[4] V. Lehmann, U. Gösele, *Adv. Mater.* **1992**, *4*, 116.
[5] M. A. Brusatori, P. R. Van Tassel, *Biosens. Bioelectron.* **2003**, *18*, 1269.
[6] O. K. Varghese, D. Gong, K. G. Ong, C. A. Grimes, *Sens. Actuators B* **2003**, *93*, 338.
[7] J. Clarke, R. Hill, D. R. Roberts, *J. Chem. Technol. Biotechnol.* **1997**, *68*, 397.
[8] A. Birner, R. Wehrspohn, U. Gösele, K. Busch, *Adv. Mater.* **2001**, *13*, 377.
[9] C. Haginoya, M. Ishibashi, K. Koike, *Appl. Phys. Lett.* **1997**, *71*, 2934.
[10] H. Masuda, M. Yotsuya, M. Asano, K. Nishio, M. Nakano, A. Yokoo, T. Tamamura, *Appl. Phys. Lett.* **2001**, *78*, 828.
[11] H. Masuda, T. Mizuno, N. Baba, T. Ohmori, *J. Electroanal. Chem.* **1994**, *368*, 333.
[12] M. Wirtz, C. R. Martin, *Adv. Mater.* **2003**, *15*, 455.
[13] D. Al Mawiawi, N. Coombs, M. Moskovits, *Jpn. J. Appl. Phys.* **1991**, *70*, 4421.
[14] M. Steinhart, J. H. Wendorff, A. Greiner, R. B. Wehrspohn, K. Nielsch, J. Schilling, J. Choi, U. Gösele, *Science* **2002**, *296*, 1997.
[15] R. Beranek, H. Hildebrand, P. Schmuki, *Electrochem. Solid-State Lett.* **2003**, *6*, B12.
[16] D. Gong, C. A. Grimes, O. K. Varghese, W. Hu, R. S. Singh, Z. Chen, E. C. Dickey, *J. Mater. Res.* **2001**, *16*, 3331.
[17] V. Zwilling, E. Darque-Ceretti, A. Boutry-Forveille, *Electrochim. Acta* **1999**, *44*, 921.
[18] O. K. Varghese, D. Gong, M. Paulose, K. G. Ong, E. C. Dickey, C. A. Grimes, *Adv. Mater.* **2003**, *15*, 624.
[19] N. Savage, B. Chwieroth, A. Ginwalla, B. R. Patton, *Sens. Actuators B* **2001**, *79*, 17.
[20] J. M. Macak, K. Sirotna, P. Schmuki, *Electrochim. Acta*, in press.
[21] J. M. Macak, P. Schmuki, unpublished results.
[22] J. B. Cotton, B. H. Hanson in *Corrosion*, *Vol. 1* (Eds.: L. L. Sheir, R. A. Jarman, G. T. Burstien), Butterworth-Heinemann, Oxford, **1994**, pp. 5–36.
[23] J. W. Schultze, M. M. Lohrengel, D. Ross, *Electrochim. Acta* **1983**, *28*, 973.
[24] M. Grätzel, *J. Photochem. Photobiol. C* **2003**, *4*, 145.
[25] A. Fujishima, K. Honda, *Nature* **1972**, *238*, 37.
[26] R. Wang, K. Hashimoto, A. Fujishima, M. Chikuni, E. Kojima, A. Kitamura, *Nature* **1997**, *388*, 431.
[27] *Titanium in Medicine* (Eds.: D. M. Brunette, P. Tengvall, M. Textor, P. Thomsen) , Springer, Berlin, **2001**, p. 1.
[28] A. Rothschild, F. Edelman, Y. Komem, F. Cosandey, *Sens. Actuators B* **2000**, *67*, 282.
[29] K. Busch, R. Wehrspohn, *Phys. Status Solidi A* **2003**, *197*, 593.
[30] J. S. Lee, M. I. Reed, R. G. Kelly, *J. Electrochem. Soc.* **2004**, *151*, B423.

